Huan Liu, Hui Zhang

An Improved DTC for In-wheel BLDC motors in Micro All-electric Vehicles

The micro all-electric vehicle pertaining to this study is rear-driven, with motors in the left and right rear wheels. The motors are brushless dc (BLDC) using Hall effect sensors with a trapezoidal back-electromotive force. The control system is developed by using a digital signal processor. To thoroughly utilize the fast torque generation feature of BLDC motors, direct torque control (DTC) is preferable, but with conventional DTC, dead-time must be added. This paper proposes an improved DTC, where the switching device operating principle is equivalent to that of a unipolar pulse width modulation (PWM) technique named PWM-ON. Dead-time is not required, and switching losses are reduced. Further analysis showed that under the improved DTC the dc supply took up only the load current, confirming that there was no return of load energy to the dc supply, which protects the batteries. Experimental results are given to confirm validity.

Key words: BLDC, dead-time, DTC, electrical vehicle, micro all-electric vehicles

Unaprijeđenje direktnog upravljanja momentom istosmjernog motora bez četkica u kotaču za mala električna vozila. Električno malo vozilo razmatrano u ovome članku ima pogon na stražnje kotače, gdje su motori smješteni u lijevi i desni stražnji kotač. Motori su istosmjerni bez četkica (BLCD) te koriste senzore zasnovane na Hallovom efektu s trapezoidalnom elektromotornom silom. Upravljački sustav razvijen je na digitalnom računalu. Kako bi se iskoristila mogućnost stvaranja bzrog momenta, što je jedno od prednosti BLCD motora, preferira se direktno upravljanje momentom (DTC), ali kod konvencionalnog DTC-a potrebno je dodati mrtvo vrijeme. U ovome članku je predložena unaprijeđena verzija DTC-a, gdje princip rada invertora isti kao i kod unipolarne pulsnoširinske modulacije (PWM-ON). U ovome slučaju mrtvo vrijeme nije potrebno te se smanjuju gubici u invertoru. Daljnja analiza je pokazala da s unaprijeđenim DTC-om nema povratka energije, što štiti baterij. Eksperimentalni rezultati su dani kako bi se potvrdila ispravnost pristupa.

Ključne riječi: istosmjerni motor bez četkica, mrtvo vrijeme, direktno upravljanje momentom, električna vozila, mala električna vozila

1 INTRODUCTION

Electric vehicles (EVs) as a solution to environment and energy problems have stimulated much research and development intended to make EVs practical [1–3]. However, EV performance is limited by the energy storage system. Although battery performance has been significantly improved, it still cannot meet the requirements of a wide variety of EVs [4]. It was found in [5] that most intercity trips in China are less than 50 km long, and that small EVs are optimal for mass adoption in the first stage of China's electric mobilization. The micro all-electric vehicle considered in this study was rear driven, with motors in the left and right rear wheels. Due to motor and battery space limitations, the vehicle used brushless motors, which also satisfied special requirements for efficiency and weight reduction.

Permanent-magnet brushless dc (BLDC) motors offer several advantages, including high efficiency, low maintenance, greater durability, compactness, and higher power density. They are commonly used in various commercial, military, and renewable energy applications. Currently, most BLDC motor control strategies use current or torque control approaches. Hysteresis current control and pulse width modulation (PWM) control, coupled with continuous control theory, are the most widely used BLDC motor control techniques [6]. Those techniques are based on the assumption that there is a linear relationship between the phase current and torque. Direct torque control (DTC) has become a powerful and popular control scheme since it was firstly proposed in the 1980s by Takahashi and Noguchi [7] and Depenbrock [8]. Due to the merits of simple structure, quick dynamic response, and robust rotor

parameters, DTC has now been extended to BLDC motor drives [9]. In [10], a lookup table for two-phase voltage selection was designed to provide faster torque response. However, dead-time compensation was still needed.

This paper proposes an improved DTC for BLDC motor operation in two-phase conducting mode. Six equivalent zero vectors were selected. Gate switching signals are equivalent to those of a unipolar PWM technique named PWM-ON. Unlike conventional DTC, there is no dead-time, reducing switching times. Under improved DTC, the dc supply takes up only the load current, protecting the batteries.

2   PWM TECHNIQUES

Fig. 1 shows a three-phase BLDC motor drive circuit with familiar feedback diodes for inductive energy recovery.
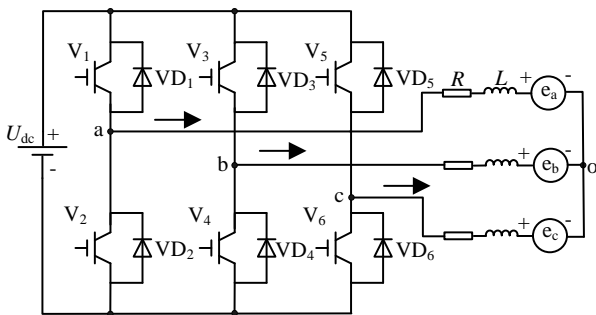
Fig. 1. Typical drive circuit of a three-phase BLDC motor

In practice, a three-phase full-wave circuit would use a PWM scheme. Fig. 2 summarizes various PWM techniques [11]. Fig. 2(a) shows a bipolar PWM technique in which both upper and lower bridge arms in one phase are controlled simultaneously by PWM signals. Usually there is a dead-time to avoid a voltage-source inverter short-circuit. Dead-times hinder improvement of the PWM frequency. Moreover, if not properly compensated for they lead to serious problems, such as waveform distortion and increased torque ripples [12–14].

The other four PWM techniques are unipolar, namely H_PWM-L_ON, H_ON-L_PWM, PWM-ON, and ON-PWM, as shown in Fig. 2(b) through (e). In unipolar PWM techniques, the PWM signal is fed to only one switch and the other switch is always off. Clearly, the upper and lower bridge arms in one phase will have no chance of being turned on simultaneously, so dead-time is not needed [15].
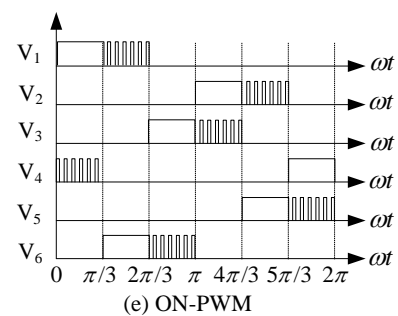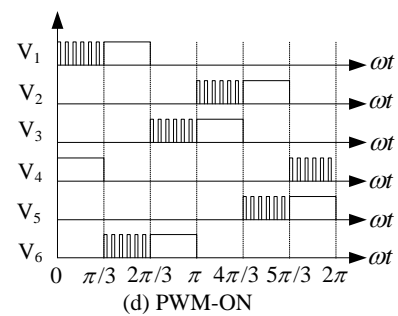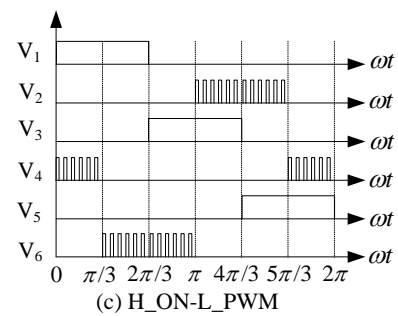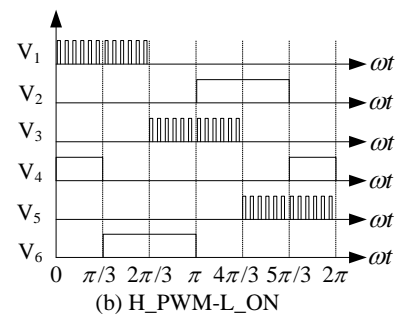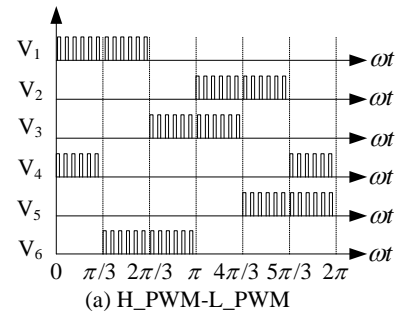
Fig. 2. Summary of various PWM techniques for BLDC motor drives

3 CONVENTIONAL DTC

3.1 Voltage space vector

As long as BLDC motor operation is characterized by sequences where both switches of a leg may be turned off simultaneously, six binary variables S_1 to S_6 are required. One binary variable represents one switch statement. Binary 1 indicates an ON state and binary 0 indicates an OFF state.

There are six active voltage vectors in a conventional two-phase conduction mode. Let us call them $\mathbf{U}_1$, $\mathbf{U}_2$, $\mathbf{U}_3$, $\mathbf{U}_4$, $\mathbf{U}_5$, and $\mathbf{U}_6$. The corresponding switching combinations $(S_1 S_2 S_3 S_4 S_5 S_6)$ are equal to (100001), (001001), (011000), (010010), (000110), and (100100) respectively. Then, zero vector $\mathbf{U}_0$ (000000) indicates six switches in the OFF state. In the $\alpha - \beta$ plane, six active voltage vectors ($\mathbf{U}_1$ to $\mathbf{U}_6$) are shown in Fig. 3. Sectors are identified by means of given combinations of three Hall effect signals (H_a, H_b, and H_c) and depicted in Table 1.
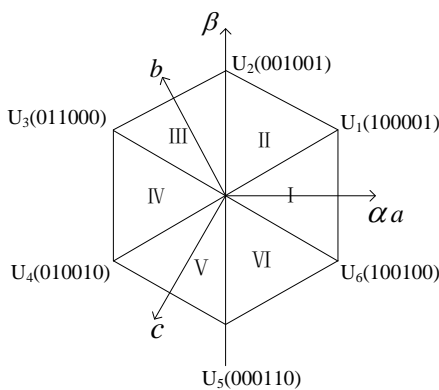
Fig. 3. Active voltage vectors in two-phase conduction mode

Table 1. Identification of six sectors in $\alpha - \beta$ plane based on Hall effect signals

$H_{(abc)}$	(110)	(010)	(011)	(001)	(101)	(100)
Sector	I	II	III	IV	V	VI

3.2 Conventional DTCs

A conventional DTC typically consists of three parts: torque and flux estimation, hysteresis comparators, and a switching table [7–9]. It has been shown that a conventional DTC operating in two-phase conduction mode is simplified to just a torque controlled drive. This is done by intentionally keeping stator flux linkage amplitude almost constant by eliminating flux control in a constant torque region [10]. Therefore, flux error φ is always selected

as zero in the voltage vector selection lookup table, and only torque error τ is used, depending on the error level of actual torque relative to reference torque. Within the hysteresis bandwidth, if actual torque is less than reference torque, torque error τ is defined as 1; if actual torque is greater than reference torque, it is -1. Details are shown in Table 2 [10].

Table 2. Voltage vector selection table proposed by Salih et al.

φ	τ	I	II	III	IV	V	VI
0	+1	$\mathbf{U}_2$(001001)	$\mathbf{U}_3$(011000)	$\mathbf{U}_4$(010010)	$\mathbf{U}_5$(000110)	$\mathbf{U}_6$(100100)	$\mathbf{U}_1$(100001)
	-1	$\mathbf{U}_5$(000110)	$\mathbf{U}_6$(100100)	$\mathbf{U}_1$(100001)	$\mathbf{U}_2$(001001)	$\mathbf{U}_3$(011000)	$\mathbf{U}_4$(010010)

In general, a BLDC motor contains two operation regions: a conduction region and a commutation region. In the conduction region, the flux linkage position remains unchanged and the three Hall effect signals do not change. The torque control signal is torque error. In the commutation region, torque error is held while the three Hall effect signals change. The torque control signal is in the flux linkage sector. Ideally, Hall effect signals can be captured and the capture interrupt is precisely estimated by the position of the flux linkage sector. Commutation is achieved by decoding position sensor signals. The space voltage vector is changed in sequence, and dead-time is not needed. Unfortunately, external noise easily interferes with Hall effect signals. Therefore, a zero-voltage vector $\mathbf{U}_0$ (000000) is applied in the commutation period. At that time, six switches are in the OFF state. Dead-time is 2 μs. In this paper we mainly consider the conduction region; the commutation region is not studied, nor are non-ideal effects of dead-time in the commutation region.

In the conduction region, a torque hysteresis comparator causes an inherently variable inverter switching frequency. An instantaneous switching period T_n of one inverter leg is defined for that inverter leg to make one complete ON-OFF-ON switching transition, as showed in Fig. 4. The inverse of T_n gives the nth instantaneous switching frequency.
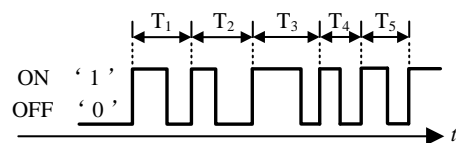
Fig. 4. Instantaneous switching period of a single inverter leg

Fig. 5 shows the typical operation of a hysteresis comparator, and gate switching waveforms when the stator flux

linkage vector is in sector I. (The torque waveform is simplified for ease of illustration.) When τ is ON (status '1'),V_3 andV_6 are conducting; otherwise, when τ is OFF (status '-1'),V_4 and V_5 are conducting. Gate switching signals are equivalent to the gate switching signals in bipolar PWM techniques. Dead-time should be considered during the transition state of either τ ON to OFF, or τ OFF to ON. Each switching period will generate two dead-time pulses.
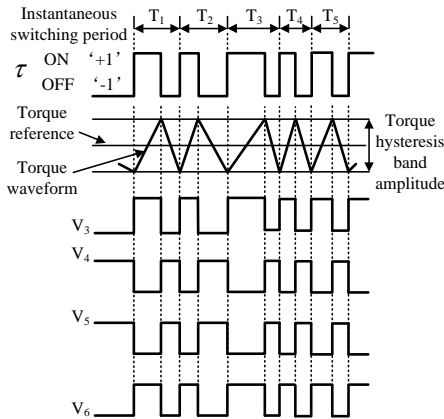
Fig. 5. Typical operation of a hysteresis comparator, and gate switching waveforms when the stator flux linkage vector is in sector I

4   PROPOSED DTC CONTAINING EQUIVALENT ZERO-VOLTAGE VECTORS

With conventional DTC, dead-time should be taken into account. Different methods have been proposed to overcome dead-time issues, such as dead-time compensation, dead-time minimization, and dead-time elimination [16]. In sector 2, the unipolar PWM technique can solve the dead-time problem. If we can obtain the voltage vectors, the switching device operating principle can be equivalent to the unipolar PWM technique. Dead-time would not be needed.

Based on the normal operation of an electrical machine, an equivalent expression for torque can be obtained by

$$T_e = k_m |\psi_r||\psi_s|\sin\theta, \qquad (1)$$

where k_m is the torque coefficient, $|\psi_r|$ is the rotor flux magnitude, $|\psi_s|$ is the stator flux magnitude, and θ is the angle between stator and rotor flux linkages.

Judging by Equation (1), a fast torque response can be obtained by adjusting the rotating speed of the stator flux linkage as quickly as possible. However, in region I of Fig. 3, for instance, in counterclockwise operation, because U_5 would force the stator flux to rotate clockwise, the associated change of torque angle would decrease too much,

causing large torque ripples. To prevent this, another vector was used instead of U_5.

In a stationary reference frame, the stator flux linkage vector can be expressed as

$$\psi_s = \int (u - Ri)dt. \qquad (2)$$

During conduction switching, the voltage vector is constant, and Equation (2) is rewritten as

$$\psi_s = ut + \int (Ri)dt + \psi_s(0), \qquad (3)$$

where $\psi_s(0)$ is the initial value of the stator flux linkage at the moment of switching.

Disregarding stator resistance, when U_0 (000000) is applied, ψ_s will stay at its original position. But θ will decrease because the magnets rotate with the rotor. So U_0 always decreases torque.

Many researchers have pointed out that U_0 is not zero. Furthermore, it has been shown that using U_0 only to decrease electromagnetic torque could have some disadvantages, such as generating more frequent and larger spikes on phase voltages, which would deteriorate the trajectory of the stator flux linkage locus, increase switching losses, and contribute to large common-mode voltages that could damage motor bearings [10].

To control electromagnetic torque smoothly, six equivalent zero vectors were selected. The rule for selecting equivalent zero-voltage vectors was obtained by analyzing voltage vectors one by one in each sector [17–20]. When the voltage space vector changes, switches should be as few as possible. Accordingly, two equivalent zero-voltage space vectors were obtained in each sector, as depicted in Table 3.

Table 3. Equivalent zero-voltage space vectors in each sector

Sector	I	II	III	IV	V	VI
Switching	(001000)	(010000)	(000010)	(000100)	(100000)	(000001)
device state	(000001)	(001000)	(010000)	(000010)	(000100)	(100000)

The most recent and best performing DTC strategy was proposed by Mourad et al. [20]. It offered improved reliability by achieving balanced switching frequencies of inverter upper and lower insulated gate bipolar transistors on the one hand, and reduction of the average value of motor common-mode voltages on the other hand. When the motor rotates counterclockwise, a vector table is selected as shown in Table 4. The same approach can be applied differently, with a permutation of the control rules of the previous approach yielding the vector selection table in Table 5.

Table 4. First vector selection table of a DTC strategy proposed by Mourad et al. for a counterclockwise rotation

τ	+1	-1
Sector I	U_2(001001)	U_0(001000)
Sector II	U_3(011000)	U_0(010000)
Sector III	U_4(010010)	U_0(000010)
Sector IV	U_5(000110)	U_0(000100)
Sector V	U_6(100100)	U_0(100000)
Sector VI	U_1(100001)	U_0(000001)

Table 5. Second vector selection table of a DTC strategy proposed by Mourad et al. for a counterclockwise rotation

τ	+1	-1
Sector I	U_2(001001)	U_0(000001)
Sector II	U_3(011000)	U_0(001000)
Sector III	U_4(010010)	U_0(010000)
Sector IV	U_5(000110)	U_0(000010)
Sector V	U_6(100100)	U_0(000100)
Sector VI	U_1(100001)	U_0(100000)
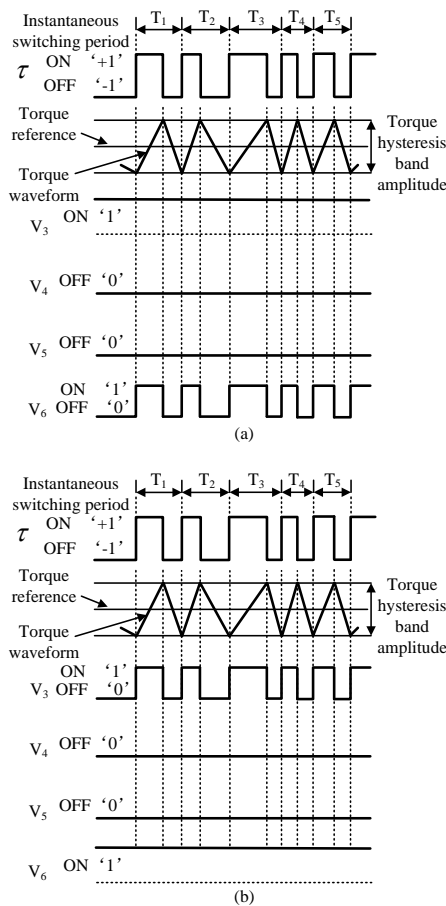
Fig. 6 shows the typical operation of a hysteresis comparator and gate switching waveforms corresponding to Tables 4 and 5 when the stator flux linkage is in region I of Fig. 3.

In Fig. 6(a), whether τ is ON (status '1') or OFF (status '-1'), V_3 is always conducting and V_4 and V_5 are not conducting; otherwise, when τ is ON, V_6 is conducting, and when τ is OFF, V_6 is not conducting. Gate switching signals are equivalent the gate switching signals in unipolar PWM techniques, namely ON-PWM.

In Fig. 6(b), when τ is ON, V_3 is conducting, and when τ is OFF, V_3 is not conducting; otherwise, whether τ is ON or OFF, V_4 and V_5 are not conducting and V_6 is always conducting. Gate switching signals are equivalent to the gate switching signals in unipolar PWM techniques, namely PWM-ON. Dead-time is eliminated.

One study [21] analyzed the influences of various unipolar PWM techniques on commutation torque ripple. They found the best mode to be PWM-ON. In this paper, the switching signal was generated by a similar PWM-ON mode. When the motor rotated counterclockwise, the vector table selected was as shown in Table 5. When the motor rotated clockwise, the vector table selected was as shown in Table 6.

Table 6. Vector selection table for a clockwise rotation

τ	+1	-1
Sector I	U_5(000110)	U_0(000010)
Sector II	U_6(100100)	U_0(000100)
Sector III	U_1(100001)	U_0(100000)
Sector IV	U_2(001001)	U_0(000001)
Sector V	U_3(011000)	U_0(001000)
Sector VI	U_4(010010)	U_0(010000)

5   SIMULATION RESULTS

The drive system was simulated for various cases, with the conventional and improved DTCs containing six equivalent zero vectors. Parameters of the motor are shown in the APPENDIX A.

Figs. 7–10 compare simulated responses to a reference speed of 200 r/min under a no-load condition and constant $T_{load} = 5$ N·m from a conventional DTC and the improved DTC. With the improved DTC, torque ripple was reduced and the dc supply current was not negative.

To show the improvement of a current waveform obtained by using the improved DTC, a harmonic analysis of the motor current was carried out. The results obtained are shown in Fig. 11. The comparison shows a reduction of low order harmonics obtained using the improved DTC.

Fig. 6. Typical operation of a hysteresis comparator and gate switching waveforms corresponding to Tables 4 and 5 when the stator flux linkage is in region I of Fig. 3.
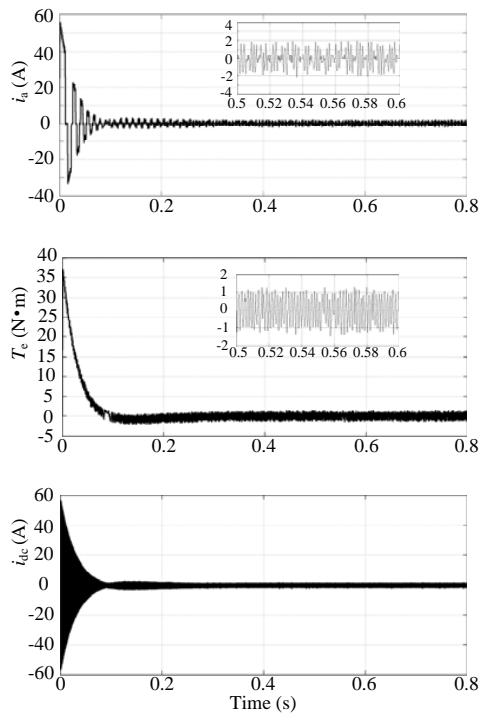
Fig. 7. Conventional DTC response to a reference speed of 200 r/min under no-load condition
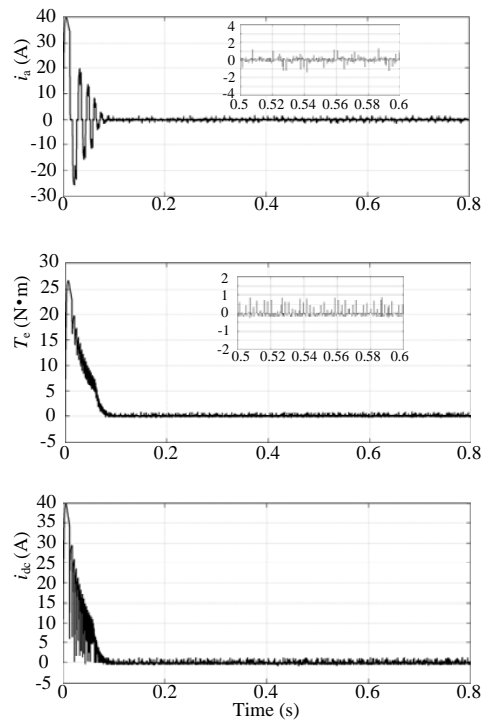
Fig. 9. Improved DTC response to a reference speed of 200 r/min under no-load condition
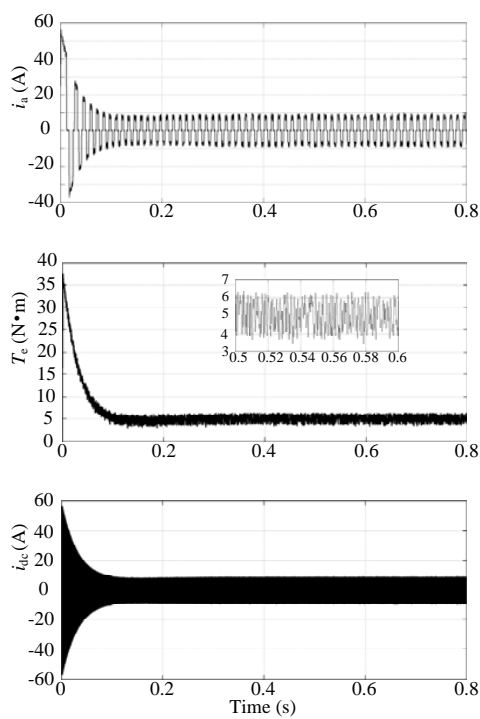
Fig. 8. Conventional DTC response to a reference speed of 200 r/min under constant $T_{load} = 5$ N·m
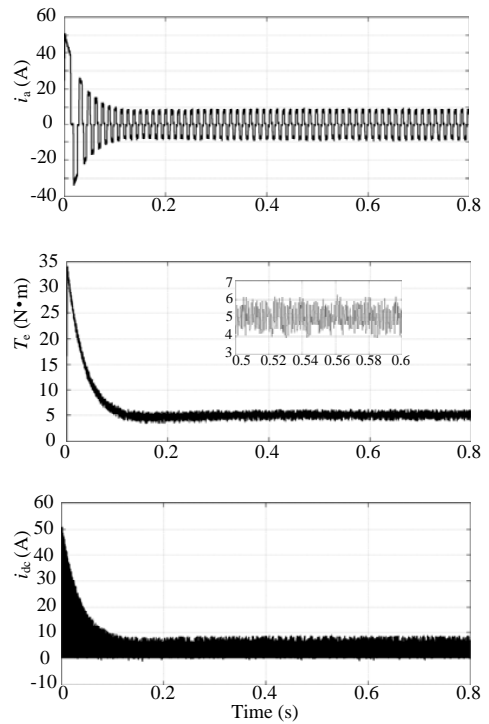
Fig. 10. Improved DTC response to a reference speed of 200 r/min under constant $T_{load} = 5$ N·m
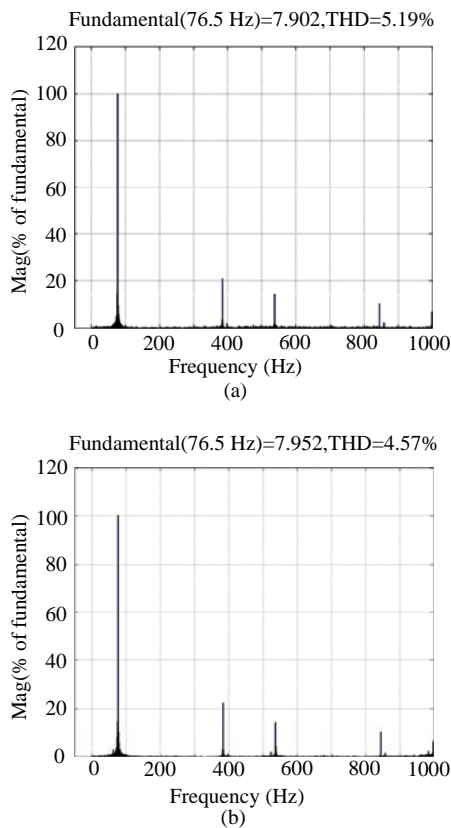
Fig. 11. *Harmonic spectrum of motor current waveform. (a) Conventional DTC. (b) Improved DTC.*
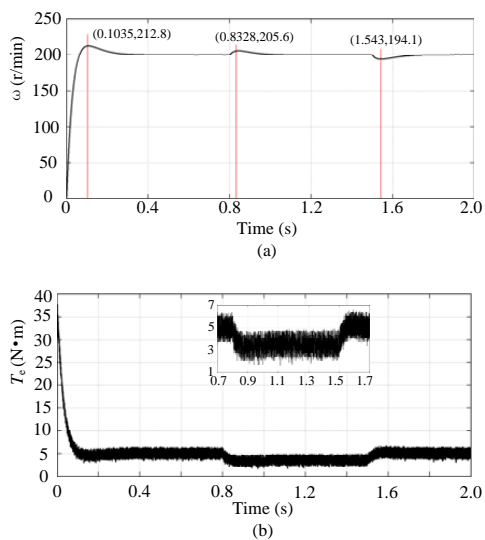
Fig. 12. *Response of conventional DTC to a reference speed of 200 r/min under load change. (a) Speed. (b) Torque.*
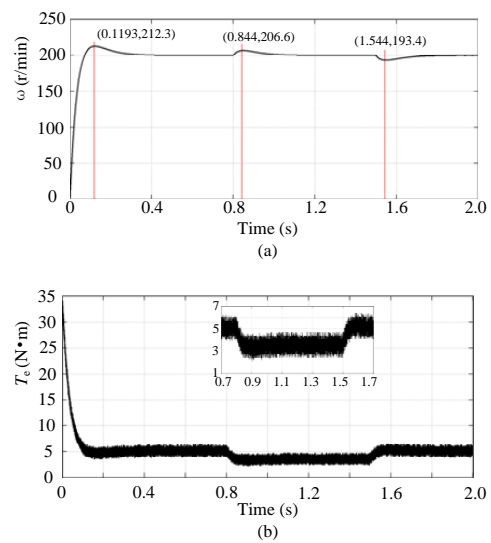
Fig. 13. *Response of improved DTC to a reference speed of 200 r/min under load change. (a) Speed. (b) Torque.*

Figs. 12 and 13 show speed and torque responses to a reference speed of 200 r/min. Initially a load of 5 N·m was applied. At 0.8 second, a load of 3.5 N·m was applied. At 1.5 second, a load of 5 N·m was applied. Initially, speed and torque tracked the reference values quickly. When the load changed, speed fluctuated and followed the reference value quickly. Torque ripple was reduced under the improved DTC.

6 EXPERIMENTAL RESULTS AND DISCUSSION

An experimental setup of a BLDC motor driving and control system was built. A Texas Instruments TMS320F28335 microcontroller was invoked as a core. The external circuit consisted of a three-phase inverter bridge, an isolated drive circuit, a position detecting circuit, and a current detection circuit. Fig. 14 shows the experimental setup.

Fig. 14. *Experimental setup of BLDC motor driving and control system*
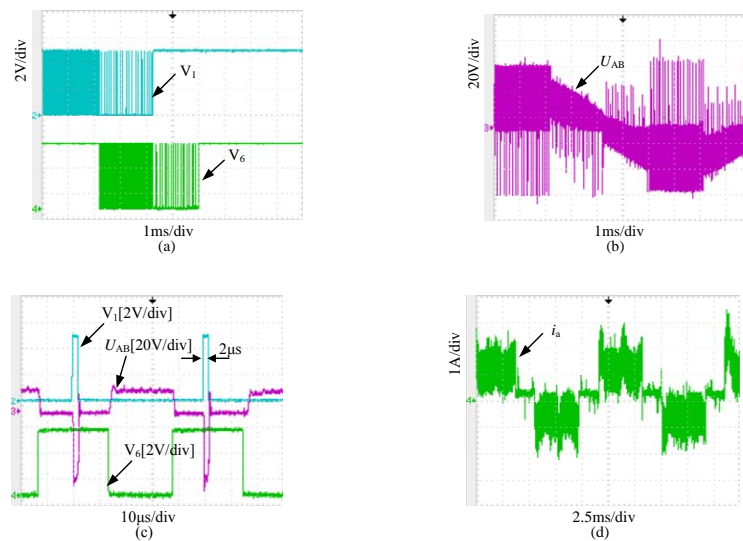
Fig. 15. (a) Waveforms of PWM signals with dead-time. (b) Output voltage waveform with dead-time. (c) Partial view of output voltage. (d) Phase-a current.
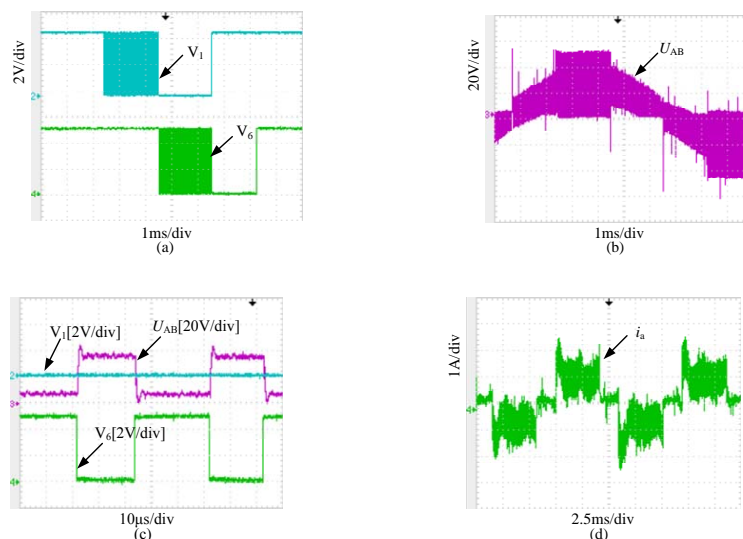
Fig. 16. (a) Waveforms of PWM signals without dead-time. (b) Output voltage waveform without dead-time. (c) Partial view of output voltage. (d) Phase-a current.

In this research, PWM current control and DTC were considered. If PWM current control was employed, PWM switching frequency was designed to be 20 kHz; otherwise, if DTC was employed, the sampling interval was 50 μs.

In PWM current control, experiments were performed with dead-time setting and without dead-time setting, separately. For comparison, two cases involved a detained PWM-ON firing mode. Experimental results are shown in Figs. 15 and 16. In Fig. 15, dead-time is 2 μs. Output volt-

age was left floating, and output current continued to flow through feedback diodes. Depending on current polarity, the reference voltage may have been delayed by dead-time. In Fig. 16, dead-time is not settled. Without dead-time, output current did not need to be conducted through feedback diodes; the dead-time effect could be eliminated.

Fig. 17 shows switching times computed for one switching device per second, both with dead-time and without dead-time. A Tektronix MD03034 mixed domain oscilloscope was used to measure switching times per sec-

ond. A Victor DM6234P+ digital tachometer was used to measure motor speed. It clearly showed that switching times with dead-time were much higher. The switching time was approximately 4,190 times per second at motor speeds from 72.5 r/min to 397.6 r/min. At the highest speed of 465.2 r/min, they were only 1,641 times per second. Without dead-time, switching times were approximately 3,430 times per second at motor speeds from 77.5 r/min to 422.4 r/min. At the highest speed of 504.7 r/min, they were 254 times per second. Therefore, it is possible to reduce switching times and minimize switching loss without dead-time. In addition, because dead-time reduced the switching device conduction time, the motor maximum speed reduced from 504.7 r/min to 456.2 r/min.
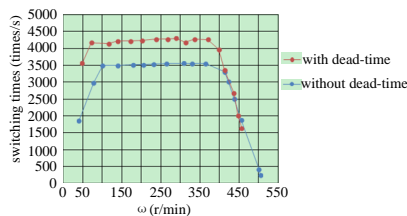
Fig. 17. Switching times computed for one switching device per second with and without dead-time

For DTC, experiments were performed with conventional DTC and with improved DTC containing six equivalent zero vectors. With conventional DTC, dead-time was 2 μs. With improved DTC, gate switching signals were generated equivalent to the gate switching signals in unipolar PWM techniques, namely PWM-ON. Dead-time was eliminated. Similar switching times results were observed, but are not listed here due to space limitations. It should be noted that switching frequency was variable, because a hysteresis loop was used for electromechanical torque.

In Fig. 18, phase-a to phase-b voltage U_{AB} and phase-a current i_a are almost the same. Details of this similarity are described in [22]. The dead-time of the inverter and the non-ideal influence of the BLDC motor were ignored in the conventional DTC. For this experiment, we assumed that the BLDC motor ran counterclockwise and flux was in region V of Fig. 3. In this study, the comparison concentrates on the instantaneous switching period.

Fig. 19 shows load voltage and load current waveforms in the instantaneous switching period for the conventional DTC. In Fig. 19(a), switching devices were switched in diagonal pairs, with V_1 and V_4 turned on and off simultaneously, and similarly for V_2 and V_3. The resultant load voltage was the difference of the pole voltages, thus U_{AB} gave a square-waveform voltage of amplitude U_{dc}. Because the BLDC motor was an inductive load, the current lagged the voltage. Fig. 19(b) shows the steady-state load current

waveform. The current was a series of exponentials, and for an interval after the load voltage reversed polarity, the instantaneous power consumption of the load was negative because voltage and current have opposite signs. This signified that stored energy in the inductive load was being returned to the dc supply through inverter feedback diodes.

The mechanism of energy feedback through the inverter can be seen by reference to the load current waveform of Fig. 19(b), where conducting devices are indicated for each portion of the switching period. At time zero, V_2 and V_3 were turned off and V_1 and V_4 were turned on, but the load current already established in the inductive load flowed for a time in the negative direction, from B to A. This negative load current flowed through feedback diodes VD_1 and VD_4 and the dc supply, thereby returning inductive load energy to the dc source.

At time t_1, when the load current fell to zero and reversed, the increasing positive current flowed through switching devices V_1 and V_4. This instant of current reversal is load dependent and can occur at any time in the half-period ($0 \sim t_2$). Consequently, switching devices must have a forward base drive throughout the half cycle so that they can take up the load current when required. However, conduction of VD_1 and VD_4 at time zero results in an immediate reversal of load voltage.

At time t_2, V_1 and V_4 were turned off and V_2 and V_3 were turned on. Positive load current continued to flow through feedback diodes VD_2 and VD_3 and the dc power supply, and load energy was again returned to the dc source.

At time t_3, when the load current fell to zero and reversed, the increasing negative current flowed through switching devices V_2 and V_3. The switching devices took up the load current.

The dc supply current waveform was a replica of the load current waveform except for the polarity reversal in alternate cycles, as shown in Fig. 19(c). Conduction of the feedback diodes clearly resulted in intervals of negative dc supply current, confirming that there was a return of load energy to the dc source during a portion of each half cycle.

Fig. 20 shows load voltage and load current waveforms for the instantaneous switching period under the improved DTC containing six equivalent zero vectors. At time zero, switching devices V_1 and V_4 were turned on, so input dc voltage (U_{dc}) was applied to the load. Increasing positive current flowed through switching devices V_1 and V_4. The dc supply took up the load current. Instantaneous power consumption of the dc supply was positive. At time t_1, V_1 was turned off. Positive load current continued to flow through feedback diodes VD_2 and V_4, and the dc supply current was zero. Therefore, instantaneous power consumption of the dc supply was zero.
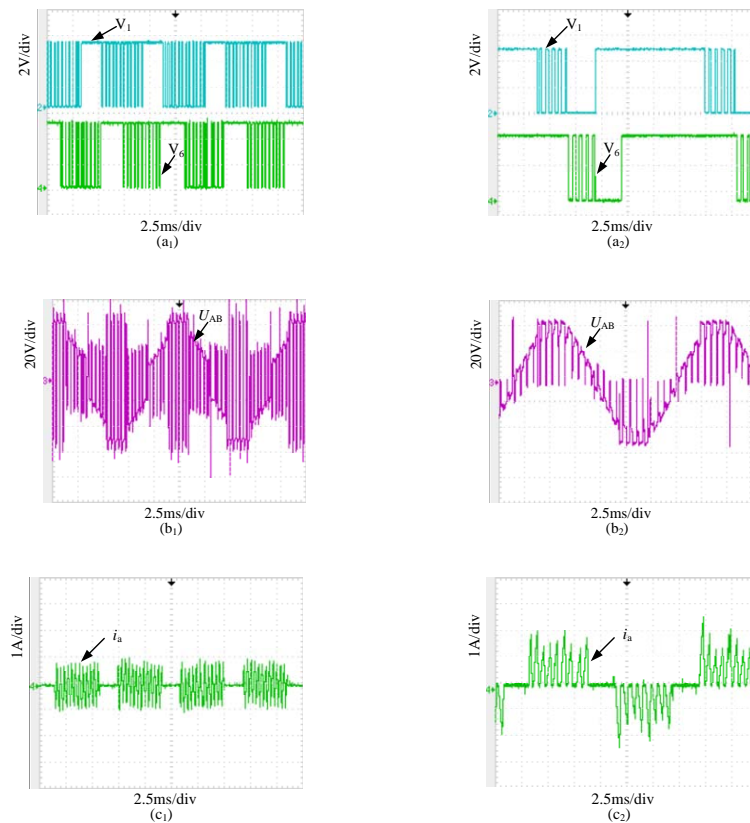
Fig. 18. Experimental waveforms under conventional DTC (subscript "1") and under improved DTC (subscript "2"). (a) Waveforms of switching devices. (b) Output voltage waveform. (c) Phase-a current.
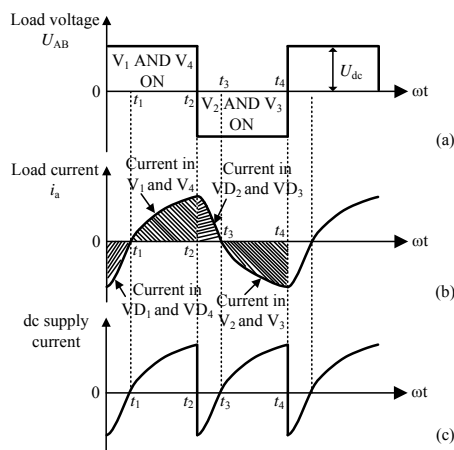
Fig. 19. Load voltage and load current waveforms in the instantaneous switching period for the conventional DTC scheme. (a) Load voltage. (b) Load current. (c) DC supply current.
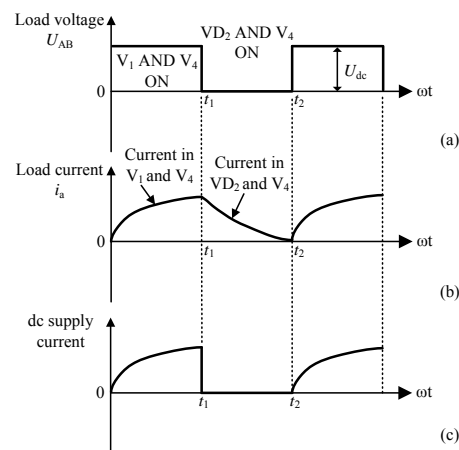
Fig. 20. Load voltage and load current waveforms in the instantaneous switching period under the improved DTC. (a) Load voltage. (b) Load current. (c) DC supply current.

From the analysis of these results it was clear that under conventional DTC, inverse-parallel rectifier diodes allowed current to reverse flow. Such feedback diodes could provide a load current reverse channel that permits load

energy through the voltage-source inverter to affect the dc supply. This would reduce the service life of the battery. By contrast, under improved DTC the dc supply takes up only the load current.

7   CONCLUSION

This paper mainly studies DTCs to be used in in-wheel BLDC motors in micro all-electric vehicles. Our research shows that under conventional DTCs dead-time must be set. The existence of dead-time leads to an increase in the number of switching times, resulting in switching loss. Therefore, dead-time compensation or eliminating the dead zone is important in conventional DTCs.

An improved DTC containing six equivalent zero vectors was evaluated, where the firing mode of the switch devices was equivalent to one of unipolar PWM techniques named PWM-ON mode. Dead-time was not necessary, solving the dead-time problem.

Further analysis showed that under a conventional DTC, conduction of feedback diodes clearly results in intervals of negative dc supply current, confirming that there is a return of load energy to the dc source during a portion of each half cycle. This reduces the service life of the battery. Under the improved DTC, the dc supply takes up only the load current, which protects the batteries.

APPENDIX A

Parameters of the BLDC motor

Rated voltage: 48 V

Rated power: 500 W

Rated speed: 500 r/min

Number of poles: 23

Resistance: 0.2 Ω

Inductance: 3.5 e-4H

ACKNOWLEDGMENT

REFERENCES

[1] A. Emadi, Y. J. Lee, and K. Rajashekara, "Power electronics and motor drives in electric, hybrid electric, and plug-in hybrid electric vehicles," *IEEE Trans. Ind. Electron.*, vol. 55, no. 6, pp. 2237–2245, 2008.

[2] X. D. Xue, K. W. E. Cheng, and N. C. Cheung, "Selection of electric motor drives for electric vehicles," in *Proc. Australasian Universities Power Engineering Conference (AUPEC)*, (Padova, Australia), pp. 1–6, Dec. 2008.

[3] R. Wang and J. Wang, "Fault-tolerant control with active fault diagnosis for four-wheel independently driven electric ground vehicles," *IEEE Trans. Veh. Technol.*, vol. 60, no. 9, pp. 4276–4287, 2011.

[4] S. M. Lukic, J. Cao, R. C. Bansal, F. Rodriguez, and A. Emadi, "Energy storage systems for automotive applications," *IEEE Trans. Ind. Elec.*, vol. 55, no. 6, pp. 2258–2267, 2008.

[5] J. Du, M. Ouyang, and H. Wang, "Battery electric vehicle parameters design targeting to cost-benefit objective," in *Proc. 8th international Conf. Vehicle Power and Propulsion Conference (VPPC).*, (Seoul, Korea (South)), pp. 1160–1164, Oct. 2012.

[6] F. Rodriguez and A. Emadi, "A novel digital control technique for brushless dc motor drives," *IEEE Trans. Ind. Electron.*, vol. 54, no. 5, pp. 2365–2373, 2007.

[7] I. Takahashi and T. Noguchi, "A new quick-response and high-efficiency control strategy of an induction motor," *IEEE Trans. Ind. Applicat.*, vol. IA-22, no. 5, pp. 820–827, 1986.

[8] M. Depenbrock, "Direct self-control (DSC) of inverter-fed induction machine," *IEEE Trans. Power Electron.*, vol. 3, no. 4, pp. 420–429, 1988.

[9] Y. Liu, Z. Q. Zhu, and D. Howe, "Direct torque control of brushless DC drives with reduced torque ripple," *IEEE Trans. Ind. Appl.*, vol. 41, no. 2, pp. 599–608, 2005.

[10] S. B. Ozturk and H. A. Toliyat, "Direct torque control of brushless dc motor with non-sinusoidal back-EMF," in *Proc. IEEE Int. Electric Machines Drives Conf. Biennial Meeting*, (Antalya, Turkey), pp. 165–171, May. 2007.

[11] Y.-S. Lai and Y.-K. Lin, "A unified approach to zero-crossing point detection of back EMF for brushless DC motor drives without current and Hall sensors," *IEEE Trans. Power Electron.*, vol. 26, no. 6, pp. 1704–1713, 2011.

[12] L. Chen and F. Z. Peng, "Dead-time elimination for voltage source inverters," *IEEE Trans. Power Electron.*, vol. 23, no. 2, pp. 574–580, 2008.

[13] D.-H. Lee and J.-W. Ahn, "A simple and direct dead-time effect compensation scheme in PWM-VSI," *IEEE Trans. Ind. Appl.*, vol. 50, no. 5, pp. 3017–3025, 2014.

[14] B. K.Bose, *Modern Power Electronics and AC Drives*. Beijing, China: China Machine Press, 2003.

[15] J. Chen and P.-C. Tang, "A sliding mode current control scheme for PWM brushless DC motor drives," *IEEE Trans. Power. Electron.*, vol. 14, no. 3, pp. 541–551, 1999.

[16] J. Yuan, Z. Zhao, B. Chen, C. Li, J. Wang, C. Tian, and Y. Chen, "An immune-algorithm-based dead-time elimination PWM control strategy in a single-phase inverter," *IEEE Trans. Power Electron.*, vol. 30, no. 7, pp. 3964–3975, 2015.

[17] Z. Li, L. Wang, S. Zhang, C. Zhang, and J.-W. Ahn, "Torque ripple reduction in direct torque controlled brushless DC motor," in *Proc. 14th international Conf. Electrical Machines and Systems (ICEMS).*, (Beijing, China), pp. 1–4, Aug. 2011.

[18] Z. Q. Zhu and J. H. Leong, "Analysis and mitigation of torsional vibration of PM brushless AC/DC drives with direct torque controller," *IEEE Trans. Ind. Appl.*, vol. 48, no. 4, pp. 1296–1306, 2012.

[19] Z. Li, S. Zhang, S. Zhou, and C. Zhang, "Direct torque control of brushless DC motor considering torque ripple minimization," *Transactions of China Electrotechnical Society*, vol. 29, no. 1, pp. 139–146, 2014.

[20] M. Masmoudi, B. E. Badsi, and A. Masmoudi, "Direct torque control of brushless DC motor drives with improved reliability," *IEEE Trans. Ind. Appl.*, vol. 50, no. 6, pp. 3744–3753, 2014.

[21] X. Zhang and B. Chen, "The different influences of four PWM modes on the commutation torque ripples in sensorless brushless DC motors control system," in *Proc. 5th international Conf. Electrical Machines and Systems (ICEMS).*, (Beijing, China), pp. 575–578, Aug. 2001.

[22] J. Murphy and F. Turnbull, *Power Electronic Control of AC Motors*. Oxford, England: PERGAMON PRESS, 1988.

Huan Liu received the B.S. degree from North University of China, Taiyuan, China, in 2002, and the M.S. degree from Southwest Jiaotong University, Chengdu, China, in 2012. He is currently working toward the Ph.D. degree in the Department of Electrical Engineering, Xi'an University of Technology, China. He is interesting in electric vehicle drive controls.

Hui Zhang received the B.S., M.S., and Ph.D. degrees from HUST in 1985, 1990, and 2002, respectively. From 2003 to 2005, he was as a Post-Doctoral researcher with XAUT and the Yongji Electric Machine Factory of China CNR Corporation. He was a Senior Visiting Scholar with Tsinghua University, China, from 2006 to 2008, and a Senior Visiting Professor with VT from 2010 to 2011. He is currently a Professor, a Ph.D. Supervisor, and an Academic Leader of Power Electronics and Power Drives with XAUT. His research interests include renewable energy generation, energy storage and control, wheel-drive electric vehicles, electric traction, and electric propulsion system.

AUTHORS' ADDRESSES
Huan Liu
Department of Electrical Engineering
Xi'an University of Technology
No. 5 Jinhua Road , 710048, Xi'an, China
email:xyliuhuan@126.com

Hui Zhang
Department of Electrical Engineering
Xi'an University of Technology
State Key Lab. of Power System
Tsinghua University
No. 5 Jinhua Road , 710048, Xi'an, China
email: zhangh@xaut.edu.cn